

0017-9310(95)00057-7

# Heat transfer and fluid flow of natural convection along a vertical flat plate in the transition region: experimental analysis of the wall temperature field

TERUMI INAGAKI

Department of Mechanical Engineering, University of Ibaraki, 12-1 Nakanarusawa 4 Chome, Hitachi, Ibaraki 316, Japan

and

KATSUO KOMORI

Department of Mechanical Engineering, Toyota National College of Technology, 2-1 Eisei Cho, Toyota, Aichi 471, Japan

(Received 27 October 1994)

**Abstract**—Heat transfer and fluid flow of natural convection along a vertical flat plate were experimentally investigated in the transition region. Local heat transfer coefficients along a vertical flat plate were measured to distinguish the first transition region. The wall temperature and fluid flow were then visualized using a liquid crystal sheet and water-soluble fluorescent paint. Also discussed are the characteristic statistical quantities with the aid of visualizations for the velocity and temperature fields. It was revealed from a series of experiments that horseshoe-shaped low-temperature patterns appear on the wall and that they play a significant role in heat transfer. When the data was ensemble-averaged it was found that the characteristic time-and-space scales of the patterns are statistically independent of not only heat flux but also the position in which they occur. Moreover, W-shaped flow patterns, which possess three-dimensional and unstable structures, appear in the near-wall region. They play a significant role in the laminar to turbulent transition.

## 1. INTRODUCTION

Initially, the boundary-layer development along a vertical flat plate is laminar not only in forced convection but also in natural convection. However, at some critical distance from the leading edge, depending on the flow fields and the thermophysical properties, small disturbances in the flow begin to become amplified, and a transition process takes place until the flow becomes turbulent. We say that various characteristic phenomena appear in the transition region. Its flow structure is inevitably different from those of the laminar and turbulent regions. The heat transfer coefficients have been measured in the turbulent natural convection boundary layer, and several empirical correlations describing heat transfer have been proposed by several workers [1–5]. The detailed mechanisms of heat and momentum transport were discussed in recent investigations [6, 7] of the turbulent natural convection boundary layer using a hot wire anemometer. A number of heat transfer experiments [8–10] of the laminar natural convection boundary layer have been performed experimentally and numerically, but the fundamental behavior of heat transfer in the transition region has not been discussed

satisfactorily. Qureshi and Gebhart [11], Gebhart [12], Gebhart and Mahajan [13] and Tanaka *et al.* [14] have analysed the transition process using linear-stability theory. However, the characteristic phenomena are not necessarily simulated by such theory. Jaluria and Gebhart [15] have investigated the flow structure in the transition region by introducing a vibrating ribbon to the laminar natural convection boundary layer. They found out that the three-dimensional and unstable structures called the longitudinal vortex system play a significant role in the laminar to turbulent transition. They also reported the W-shaped flow structure in the near-wall region through the measurement of the spanwise velocity distribution using a hot wire anemometer. The longitudinal vortex pairs lie between adjacent maxima and minima of the spanwise velocity distribution. However, this is not natural transition but artificial transition. It is important to discuss more essential transition processes based on the natural phenomena. Fujii [16] has experimentally investigated the criteria of the transition region under constant wall temperature. Fujii *et al.* [5] have also visualized the lateral structure of the transition region using the mirage technique. They found out that several lateral vortex pairs appear in the near-wall region

## NOMENCLATURE

$A$	surface area of the heat transfer plate [m <sup>2</sup> ]	$T_w$	wall temperature [K]
$g$	gravitational acceleration [m s <sup>-2</sup> ]	$T_\infty$	environment temperature [K]
$H$	length from the leading edge of the heat transfer plate [m] occurring position of a horseshoe-shaped low-temperature pattern [m]	$V$	electric voltage for power supply [V]
$HW$	streamwise distance between vertically aligned horseshoe-shaped low-temperature patterns [m]	$W$	spanwise length of a horseshoe-shaped low-temperature pattern [m].
$Gr_H^*$	modified Grashof number $g\beta q_w H^4 / \kappa \nu^2$	Greek symbols	
$h_H$	local heat transfer coefficient [W m <sup>-2</sup> K <sup>-1</sup> ]	$\alpha$	thermal diffusivity of fluid [m <sup>2</sup> s <sup>-1</sup> ]
$I$	electric current for power supply [A]	$\beta$	coefficient of volume expansion of fluid [K <sup>-1</sup> ]
$L$	streamwise length of a horseshoe-shaped low-temperature pattern [m]	$\Delta T$	temperature difference between the wall and environment $T_w - T_\infty$ [K]
$N$	number of data	$\kappa$	thermal conductivity of fluid [W m <sup>-1</sup> K <sup>-1</sup> ]
$Nu_H$	local Nusselt number $h_H H / \kappa$	$\nu$	kinematic viscosity of fluid [m <sup>2</sup> s <sup>-1</sup> ]
$Pr$	Prandtl number $\nu / \alpha$	$\nu_w$	kinematic viscosity of fluid based on wall temperature [m <sup>2</sup> s <sup>-1</sup> ]
$q_w$	wall heat flux [W m <sup>-2</sup> ]	$\nu_\infty$	kinematic viscosity of fluid based on environment temperature [m <sup>2</sup> s <sup>-1</sup> ]
$Ra_H^*$	modified Rayleigh number $Gr_H^* Pr$	$\sigma$	standard deviation.
$T_p$	passage time of a horseshoe-shaped low-temperature pattern [s]	Superscript	
$T_R$	life span of a horseshoe-shaped low-temperature pattern [s]	—	ensemble-averaged value.

and they play a significant role in heat transfer. However, it is important to analyse the temperature field simultaneously in addition to the velocity field.

A few studies, as mentioned above, have been performed; however, several problems still remain to be analysed in the transition region of natural convection and compansion needs to be made with laminar and turbulent flows. In this region the velocity field has been investigated by using flow visualizations (for instance Fujii *et al.* [5]) and quantitative measurements (for instance Jaluria and Gebhart [15]). However, the front view of the near-wall region has not been visualized. It is important to make clear the spanwise flow structure in addition to the lateral one. The wall temperature field is not discussed in considerations of what kind of temperature pattern is generated on the wall and what kind of relation between heat transfer and temperature pattern exists. Even if a liquid crystal sheet displaying an optimum color in a range of temperature is used, various wall heat fluxes can be attained according to the temperature of the environment. That is, we can learn more about the phenomena of a comparatively wide scope. Moreover, the time-and-space structures of the wall temperature pattern have not been scaled quantitatively or statistically. Such scaling is important in the transition region to develop a new structural modeling based on the experimental results. However, a database to be applied to the modeling has not been proposed. It is also necessary to clarify an influential

factor of the characteristic flow and temperature patterns by introducing statistical treatment.

In the present study, therefore, heat transfer and fluid flow of natural convection along a vertical flat plate were experimentally investigated in the transition region. This flow system is the most suitable in estimating the fundamental behavior of buoyancy and the wall effect, because the generated flow along a flat plate acts in the buoyant direction. We adopted water as the working fluid to visualize the characteristic behavior. Under various wall heat flux conditions, local heat transfer coefficients along a vertical flat plate were measured initially using a thermocouple to classify the transition region. The wall temperature field was then visualized using a liquid crystal sheet and was analysed by a color digital image processing unit. The two-dimensional flow structure in the near-wall region was also discussed by means of flow visualization using a water-soluble fluorescent paint. This was performed to support the thermal visualization. Furthermore, we can observe the temperature and velocity fields simultaneously by combining two types of visualizations. As far as the authors know, this is the first experiment based on simultaneous visualization. We also estimated the statistical quantities in the streamwise and spanwise directions to discuss the detailed transport mechanisms. The statistical treatment is based on the data obtained by a series of thermal visualizations. We focused on the near-wall time-and-space structures.

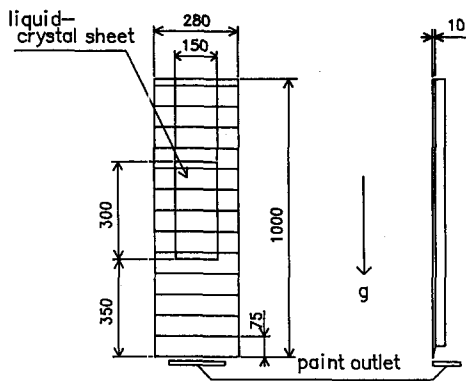


Fig. 1. A schematic illustration of the present apparatus.

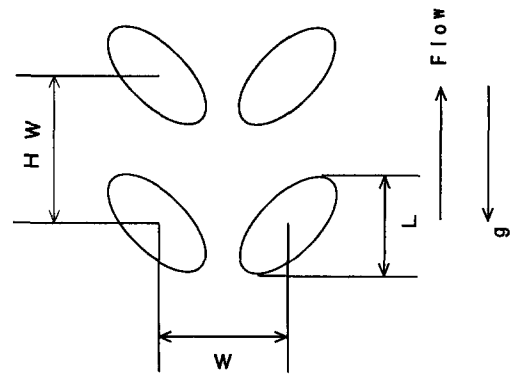


Fig. 2. A concept model for a definition of space scale.

## 2. EXPERIMENTAL APPARATUS AND MEASUREMENT

A schematic illustration of the experimental apparatus is presented in Fig. 1. The vertical plate is composed of a bakelite plate with dimensions 10 mm in thickness, 280 mm in width and 1000 mm in length. The heaters are composed of stainless foils with dimensions  $30\ \mu\text{m}$  in thickness, 75 mm in width and 280 mm in length. These heaters are glued on the surface of the bakelite plate and are connected in series. They were heated by an AC power supply to obtain a uniform heat flux throughout the test surface. The wall temperatures were measured using chromel–alumel thermocouples of  $70\ \mu\text{m}$  diameter. The thermocouples are spot welded on the back of the heater at 20 mm intervals along the central vertical line. The expanded polystyrene plate of 50 mm thickness is furnished to the back of the bakelite plate. Heat loss by thermal radiation is negligibly small as compared with convective heat transfer, because the difference between the wall and environment temperatures is within  $25^\circ\text{C}$  throughout all experiments. The heat loss by thermal conduction and thermal radiation is estimated to be less than 3.5% of the total wall heat flux. The wall heat flux was therefore calculated from an electric input to the heater. Two side walls of 200 mm width are attached on the side of the heat transfer plate to reduce the influence of the surroundings. The leading edge is made up of an acute angle of  $60^\circ$  to realize a smooth development of the boundary layer. The heat transfer plate was vertically set up and was submerged into a large rectangular reservoir tank with dimensions 2000 mm high, 1000 mm wide and 800 mm deep. The reservoir tank is full of water. A series of experiments started 24 h after filling with water. It is important to maintain as small a fluctuating intensity of the environment as possible when the transition region is measured.

The wall temperatures were visualized using a liquid crystal sheet glued on the test surface in the transition modified Rayleigh number,  $Ra_{\text{tr}}^*$ , region. The utilized liquid crystal sheet displays various colors in the range of  $40 \pm 2.5^\circ\text{C}$  according to wall temperature. Its size

is 300 mm long, 150 mm wide and  $100\ \mu\text{m}$  thick (including a  $50\ \mu\text{m}$  thick polyester film). In measuring, the wall heat flux was therefore adjusted to display optimum colors on the liquid crystal sheet. The observation field was lit up using two photo-reflector lamps (500 W) from two sides at an angle of  $45^\circ$ . These patterns were recorded by video recorder and were analysed using a color digital image processing unit. The sampling interval is 0.1 s in the digital image acquisition process. Several statistical quantities for visualized data were then calculated by Engineering Work Station (HP-MODEL 715/33). Note that the liquid crystal sheet is removed when the heat transfer coefficients are measured. The two-dimensional flow structure in the near-wall region was also visualized by a red or green colored water-soluble fluorescent paint. As illustrated in Fig. 1, the tracer flows out from the slit-shaped rectangular opening attached just before the leading edge of the heat transfer plate. The opening area is  $200 \times 0.5\ \text{mm}$ . We can obtain the two-dimensional and uniform flow pattern by applying these devices.

Furthermore, we investigated the characteristic behavior in the transition region by introducing the following physical quantities based on the thermal visualization using a liquid crystal sheet. Figure 2 illustrates the concept model for a measurement target which gives a characteristic low-temperature pattern. A definition of the physical quantities for the space scale is schematically recognized from this figure. In the color digital image processing unit a temperature on the liquid crystal sheet is expressed as a brightness value. As shown in Fig. 2, a space scale can be obtained by counting picture elements between the locations with an object brightness value. By applying this procedure,  $W$  can be defined as the spanwise length between the lowest temperature locations in a low-temperature pattern,  $L$  is the streamwise length of a low-temperature pattern, and  $HW$  is the streamwise distance between the lowest temperature locations of two vertically aligned low-temperature patterns. Figure 3 illustrates the concept models for a definition of the time scales. As shown in Fig. 3, a time scale can be

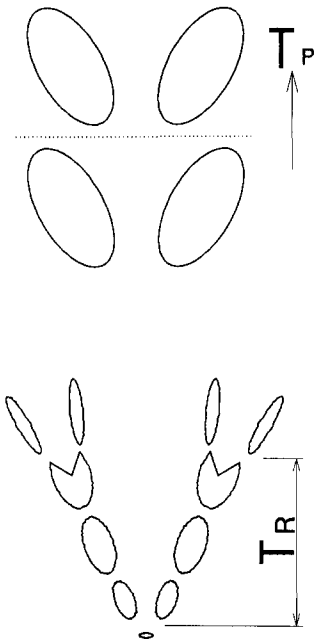


Fig. 3. A concept model for a definition of time scale.

obtained by a counting period during this transient process.  $T_R$  is the life span from the appearance until the collapse of a low-temperature pattern.  $T_P$  is the passage time when a low-temperature pattern passes through at a fixed position. Note that the space scales and the passage time were measured at an intermediate time of the life span. A number of low-temperature patterns appear on the wall repeatedly. There is a need to extract the characteristic quantities from a number of patterns. We adopted an ensemble-averaged value among space and time scales. The ensemble-average is based on the total number of the measured data under a wall heat flux. We defined these parameters as the characteristic quantities which are representative of the space-and-time structures in the transition region.

The influence of thermophysical properties on heat transfer is negligible, because the temperature difference,  $\Delta T = (T_w - T_\infty)$ , between the wall and environment temperatures is within 25°C throughout all experiments. The thermophysical properties were estimated at their mean temperature,  $(T_w + T_\infty)/2$ . Moreover, errors of experimental data were estimated using uncertainty analysis based on ANSI/ASME PCT 19.1–1985 [17].

### 3. RESULTS AND DISCUSSION

#### 3.1. Heat transfer

Local heat transfer coefficients of natural convection along a vertical flat plate were measured to confirm the applicability of the heat transfer plate to a series of experiments. We also classified the transition region through the heat transfer measurement. The

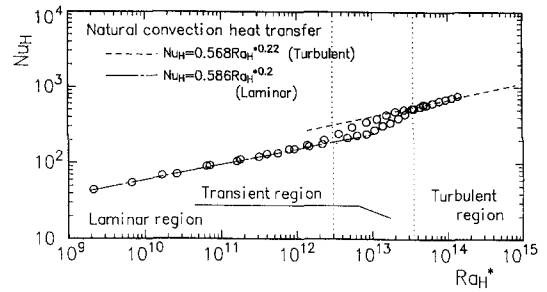


Fig. 4. Local Nusselt numbers for the laminar, transition and turbulent regions.

measured data are illustrated in Fig. 4 along with two empirical correlations. The ordinate is local Nusselt number,  $Nu_H$ , and the abscissa is  $Ra_H^*$ . The dashed-and-dotted line for the laminar region presents the empirical correlation defined in the following form [18]

$$Nu_H = \left( \frac{Pr}{4 + 9\sqrt{Pr} + 10Pr} \right)^{1/5} \left( \frac{v_\infty}{v_w} \right)^{0.17} Ra_H^{*1/5}. \quad (1)$$

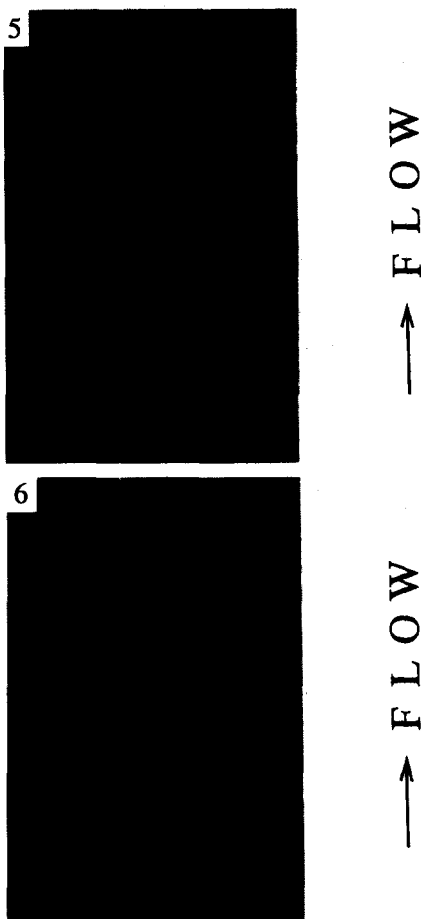
The coefficient on the right-hand side, including the influence of thermophysical properties, was estimated at about 0.586 for the laminar region. The dashed line for the turbulent region stands for the empirical correlation proposed by Vliet and Liu [2], who investigated heat transfer of turbulent natural convection along a uniformly heated vertical flat plate using water as working fluid

$$Nu_H = 0.568 Ra_H^{*0.22}. \quad (2)$$

Since the measured data for the laminar and turbulent regions are well correlated with these empirical correlations, the authors confirmed that the experimental apparatus is adequate to develop the following discussion. It is obvious from this figure that the measured data are widely distributed in the transition region. It is also clear that the behavior of heat transfer in the transition region is different from that for the laminar and turbulent regions. On the basis of the heat transfer experiments, the transition region can be classified when  $Ra_H^* = 3.0 \times 10^{12} - 3.5 \times 10^{13}$ . Therefore, the following experiments were performed in these regions.

#### 3.2. Thermal visualization on the wall

The color pattern on the liquid crystal sheet varies according to wall temperature. It is desirable that the time response of its color change is smaller than the true temperature change to keep a reliability of the measured data. Its observation time-constant [19] is estimated to be about 0.5 s when the temperature difference between wall and environment is 25°C. Note that the maximum width of fluctuating wall temperature is about 3.5°C. We therefore confirmed that the liquid crystal sheet is adequate for discussing a



Figs. 5 and 6. Two-dimensional wall temperature pattern visualized by liquid crystal sheet.

time scale. The thermal visualizations were performed in the range of  $Ra_{\text{H}}^* = 3.0 \times 10^{12} - 3.5 \times 10^{13}$ .

We will explain the way of looking at a series of visualized photographs using a liquid crystal sheet. The black color regions are representative of high-temperature regions. These regions show that the heat transfer coefficients are locally small in comparison with the surroundings on the wall, because the heat transfer plate is heated uniformly. The dark color regions are representative of low-temperature regions. The local heat transfer coefficients will always be large in these regions. As far as the authors know, only Kitamura *et al.* [20] have visualized a similar pattern using a liquid crystal sheet in the transition region of natural convection along a uniformly heated vertical flat plate. However, they have not systematically investigated and analysed wall temperature.

The wall temperature patterns shown in Figs. 5 and 6 are the typical patterns in the transition region. We named these patterns horseshoe-shaped low-temperature patterns. Although these patterns appear on the wall repeatedly, several temperature patterns, as illustrated in Figs. 7 and 8, do sometimes also appear. That is, it is obvious from Fig. 7 that several vertically aligned horseshoe-shaped low-temperature patterns

are generated. Furthermore, two horizontally aligned horseshoe-shaped low-temperature patterns can be observed, as shown in Fig. 8.

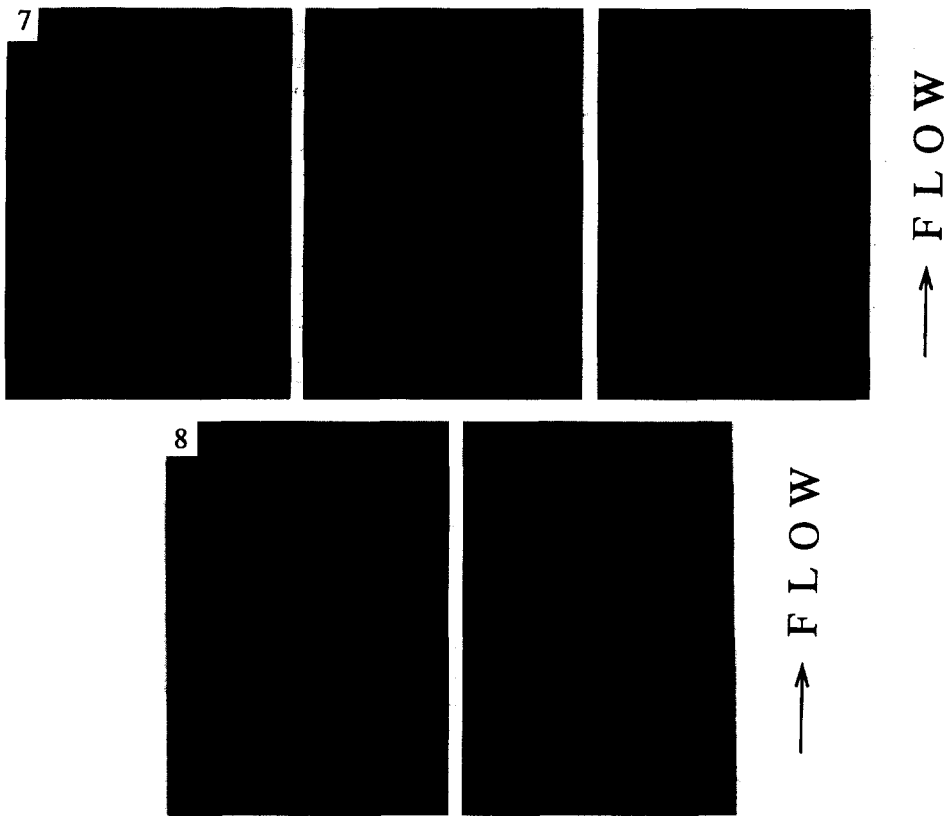
On the other hand, Fig. 9 indicates the transient photographs which represent a typical process from the appearance until the collapse of a horseshoe-shaped low-temperature pattern. The observation time interval of these photographs is 0.5 s. A horseshoe-shaped low-temperature pattern suddenly appears just downstream of the small low-temperature regions as shown in Figs. 5 and 6. This small region will be the origin of a horseshoe-shaped low-temperature pattern. However, it does not occur at a fixed location on the wall. An occurring location of these characteristic patterns is widely distributed in the range of  $Ra_{\text{H}}^* = 3.0 \times 10^{12} - 3.5 \times 10^{13}$ . We cannot easily discriminate its occurring location. It is therefore necessary to discuss the statistical characteristics. Individual horseshoe-shaped low-temperature patterns then begin to collapse into more than two complicated parts after displaying dark color. We defined this period as the life span. Turbulent transition is generated on the wall through a series of transient motions. That is, as illustrated in Fig. 3, the flow becomes turbulent during a divergence process of the low-temperature pattern. The horseshoe-shaped low-temperature pattern disappears in the turbulent region and it becomes irregular on the wall.

The temperature of a horseshoe-shaped pattern is low compared with the surroundings on the wall. The existence of a low-temperature pattern means that a low-temperature fluid lump penetrates to the near-wall region and that it exchanges heat between wall and environment. The low-temperature fluid lump is supplied from the outside of the boundary layer. Therefore, we presumed that heat exchange is taking place between wall and environment during the life span of the horseshoe-shaped low-temperature pattern.

### 3.3. Near-wall flow visualization

The above-mentioned two-dimensional thermal visualization is not sufficient to discuss the detailed flow structure. The origin of the horseshoe-shaped low-temperature pattern cannot necessarily be explained. However, we can discuss the flow structure relating to heat transfer with the aid of the two-dimensional flow visualization using a water-soluble fluorescent paint. Moreover, we can observe the temperature and velocity fields simultaneously by combining two types of visualizations. The flow visualizations were performed in the range of  $Ra_{\text{H}}^* = 3.0 \times 10^{12} - 3.5 \times 10^{13}$ .

The visualized spanwise flow patterns in the near-wall region are illustrated in Figs. 10 and 11. As shown in these figures, several characteristic and complicated horseshoe-shaped flow patterns can be observed. We named them the W-shaped flow pattern, which is similar to the W-shaped spanwise velocity distribution measured by Jaluria and Gebhart [15]. We can con-



Figs. 7 and 8. Two-dimensional wall temperature pattern visualized by liquid crystal sheet [two vertically (7) and horizontally (8) aligned horseshoe-shaped low-temperature patterns].

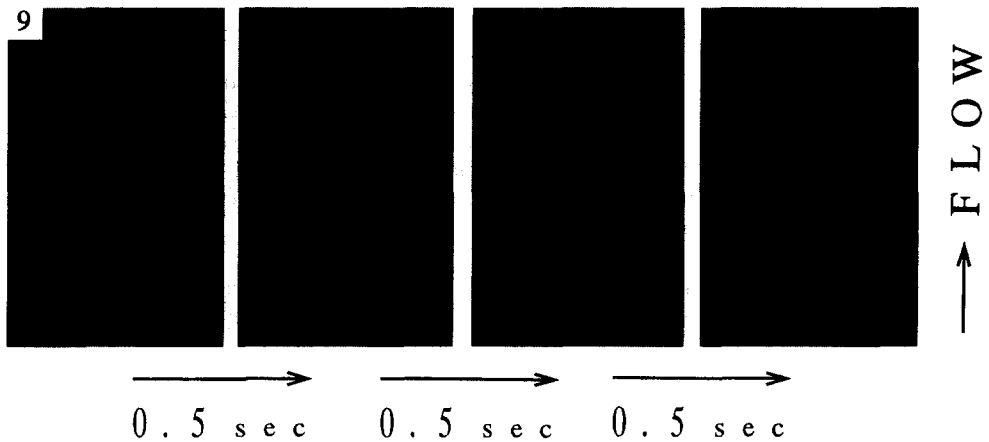
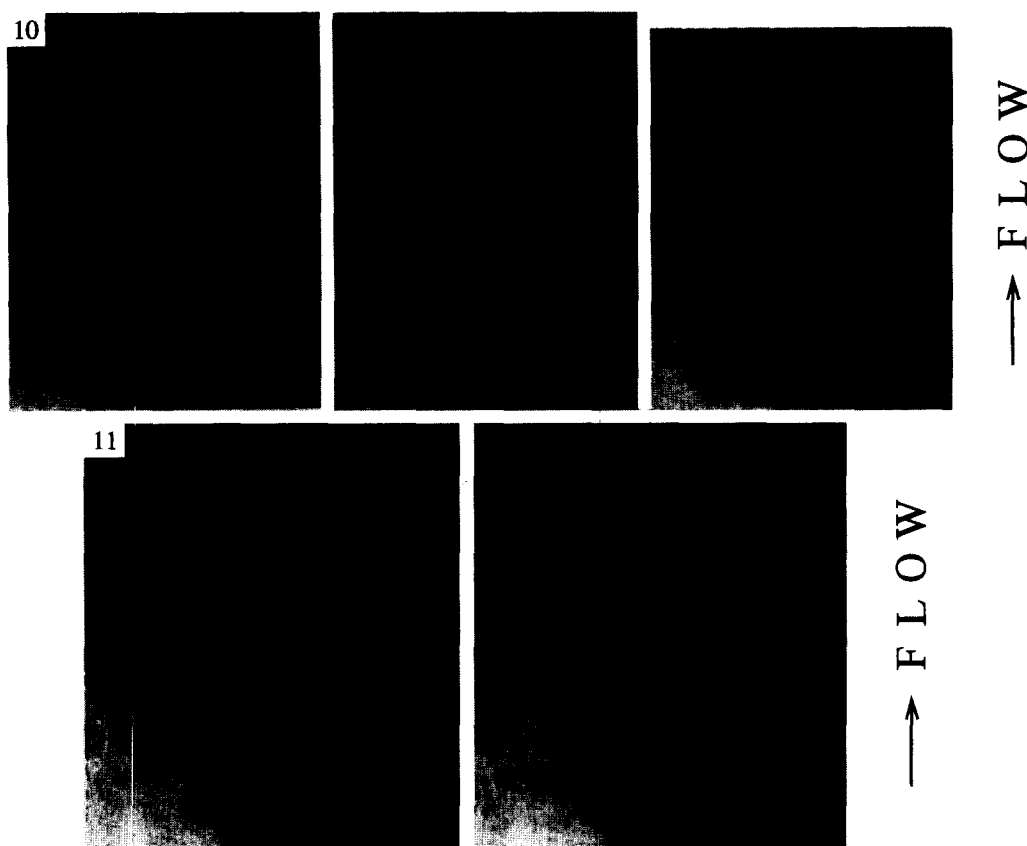


Fig. 9. Two-dimensional transient motion of a single horseshoe-shaped low-temperature pattern.

firm the existence of such characteristic patterns from observing a front view of the wall. The positions where this flow pattern occurs correspond to the transition region classified by the heat transfer measurement. Therefore, we confirmed that the tracer itself does not affect a transition process. As pointed out by Jaluria and Gebhart [15], it is assumed that the W-shaped flow pattern is generated by a spanwise velocity difference.

By combining two types of visualizations, it is

revealed that a high-speed fluid motion occurs in the black region representing high-temperature. On the other hand, low-speed fluid motion occurs in the dark color region representing low-temperature. As is shown in the thermal visualization, the high-temperature region appears at the central position in a horseshoe-shaped low-temperature pattern. From the flow visualization, we can also confirm that the high-speed fluid motion appears at the central position in a W-shaped flow pattern. The normal ejection of a



Figs. 10 and 11. Two-dimensional near-wall flow structure visualized by water-soluble fluorescent paint.

couple of vortices, which are rotating in opposite directions to each other, symmetrically start at this position. This motion ejects to the outer region as shown in Fig. 10. Furthermore, it is revealed that the low-temperature-and-velocity and high-temperature-and-velocity fluid motions are combined in these W-shaped flow patterns. We presumed that the scale of the three-dimensional structure of these patterns is rather large, because the visualized two-dimensional scale is comparatively large. However, a more effective visualization technique needs to be performed to find out the three-dimensional behavior of the W-shaped flow pattern. The authors only investigated the thermal structure in the transition region with the aid of two-dimensional flow visualization.

As mentioned in Section 3.2, several horseshoe-shaped low-temperature patterns simultaneously occur on the wall. We also confirmed from Fig. 11 that a W-shaped flow pattern appears and collapses repeatedly at various locations. Initially, as is illustrated in Fig. 10, an unstable wave occurs just upstream of a W-shaped flow pattern. The unstable wave corresponds to the small low-temperature region shown in Figs. 5 and 6. We presumed that the W-shaped flow pattern will be generated by an instability such as the unstable wave. Then, a wavy flow pattern becomes turbulent after transforming into a W-shaped flow pattern. That is, the turbulent transition

takes place during this transient process. Consequently, we also defined this period as the life span of a W-shaped flow pattern. This pattern disappears in the turbulent region and a flow pattern becomes irregular. Although the relation between the present pattern and the lateral structure [5] is not necessarily obvious, it is assumed that the front view of the lateral structure corresponds to the present pattern.

We confirmed through the flow visualization that the visualized W-shaped flow pattern possesses three-dimensional and unstable structures. The low-temperature-and-velocity and high-temperature-and-velocity fluid motions are combined in this pattern. We also presumed from a series of visualizations that the horseshoe-shaped low-temperature patterns are generated by the W-shaped flow pattern. In its appearance and collapse process, heat exchange is taking place between wall and environment. Therefore, heat transfer coefficients begin to become amplified in the transition region as compared with those of the laminar region.

#### 3.4. Characteristic statistical quantity

In this section a statistical behavior of the horseshoe-shaped low-temperature pattern is discussed by the definition mentioned in Section 2. Figure 12 illustrates the spanwise length,  $W$  (m), of a horseshoe-shaped low-temperature pattern. The abscissa is the

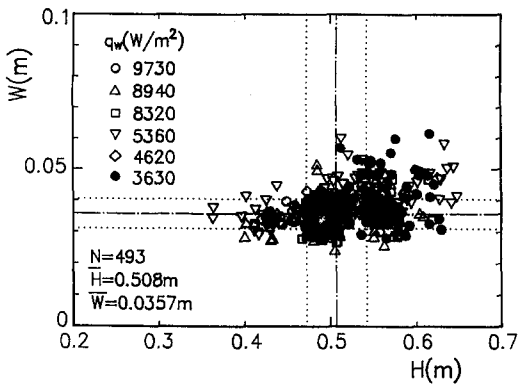


Fig. 12. Spanwise length of a horseshoe-shaped low-temperature pattern.

occurring position,  $H$  (m), which is a distance from the leading edge of the heat transfer plate. The streamwise length,  $L$  (m), and the passage time,  $T_p$  (s), of a horseshoe-shaped low-temperature pattern are shown in Figs. 13 and 14 vs  $H$  (m). The dotted lines in these figures illustrate the standard deviations of these data, and the dashed-and-dotted lines show their ensemble-averaged values. It is revealed from these figures that the time-and-space scales of a horseshoe-shaped low-

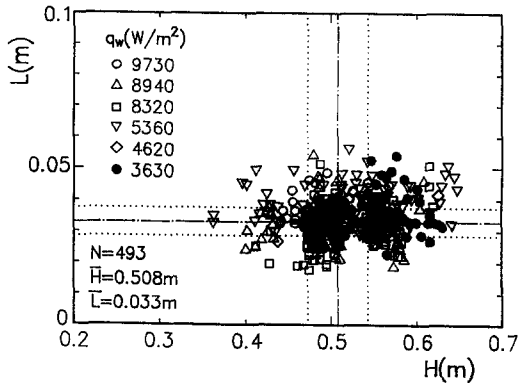


Fig. 13. Streamwise length of a horseshoe-shaped low-temperature pattern.

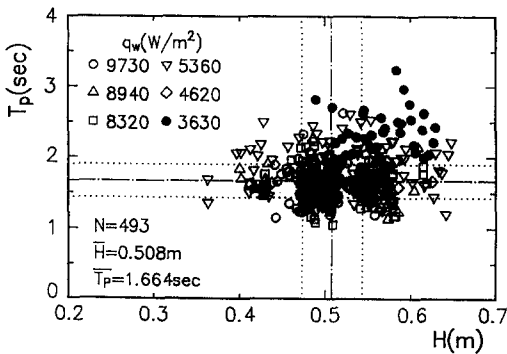


Fig. 14. Passage time of a horseshoe-shaped low-temperature pattern.

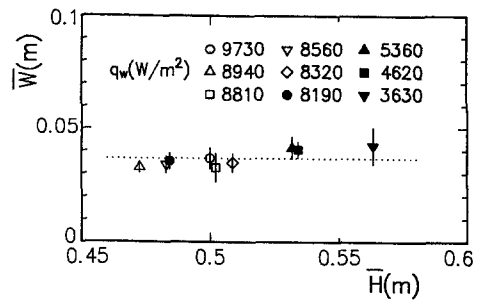


Fig. 15. Ensemble-averaged spanwise length of a horseshoe-shaped low-temperature pattern.

temperature pattern are widely distributed on the wall in the transition region. That is, these raw data vary widely. Small fluctuating motions, which are coalescing with each other in the flow, become amplified at some critical points. We presumed that the characteristic temperature and flow patterns are generated by them. The energy needed to make such patterns is different in each case owing to the irregularity of the individual small fluctuating motions. The time-and-space scales, not ensemble-averaged, are therefore fluctuating. The characteristic temperature and flow patterns, which play a significant role in heat transport, appear and disappear anywhere in the transition region. We therefore presume that the heat transfer coefficients are widely distributed in the transition region.

Furthermore, we adopted the ensemble-averaged value to investigate the statistical behavior of the transition region in the following figures. The ensemble-averaged values are based on 50–80 data. Figure 15 shows the ensemble-averaged spanwise length,  $\bar{W}$  (m), with wall heat flux,  $q_w$  ( $\text{W m}^{-2}$ ), as a parameter. The abscissa is the ensemble-averaged occurring position,  $\bar{H}$  (m). The ensemble-averaged streamwise length,  $\bar{L}$  (m), is illustrated in Fig. 16 vs  $\bar{H}$  (m) and  $q_w$  ( $\text{W m}^{-2}$ ). The ensemble-averaged passage time,  $\bar{T}_p$  (s), is shown in Fig. 17 vs  $\bar{H}$  (m) and  $q_w$  ( $\text{W m}^{-2}$ ). Figure 18 indicates the ensemble-averaged life span,  $\bar{T}_R$  (s), with  $q_w$  ( $\text{W m}^{-2}$ ) as a parameter. The abscissa is  $\bar{H}$  (m). The present time data possess about 10–15% time delay as compared with the phenomena observed by the

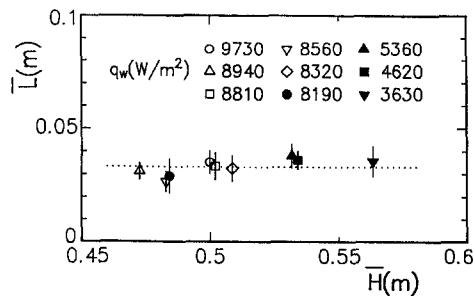


Fig. 16. Ensemble-averaged streamwise length of a horseshoe-shaped low-temperature pattern.

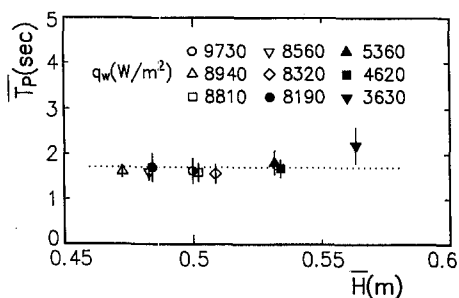


Fig. 17. Ensemble-averaged passage time of a horseshoe-shaped low-temperature pattern.

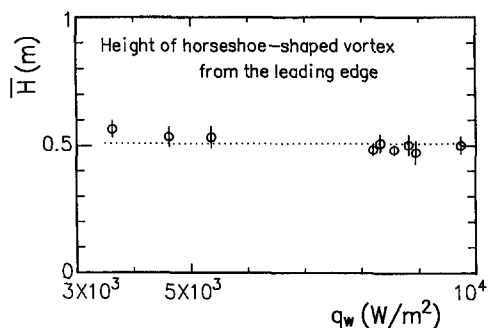


Fig. 20. Ensemble-averaged occurring position from the leading edge of the heat transfer plate.

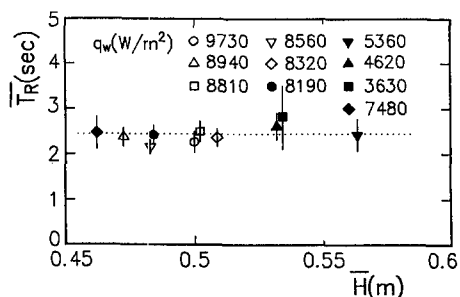


Fig. 18. Ensemble-averaged life span of a horseshoe-shaped low-temperature pattern.

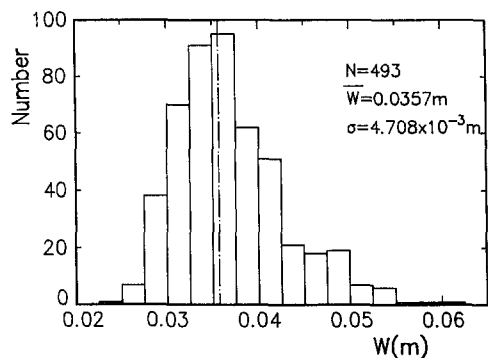


Fig. 21. Histogram for the spanwise length of a horseshoe-shaped low-temperature pattern.

flow visualization using a water-soluble fluorescent paint, because the observation time-constant of the liquid crystal sheet is estimated to be about 0.5 s. The ensemble-averaged streamwise distance,  $\overline{HW}$  (m), between vertically aligned horseshoe-shaped low-temperature patterns, is plotted with  $q_w$  ( $W m^{-2}$ ) in Fig. 19. It is obvious from this figure that the horseshoe-shaped low-temperature patterns align regularly in the streamwise direction.  $\overline{H}$  (m) is also plotted with  $q_w$  ( $W m^{-2}$ ) in Fig. 20. It is clear from this figure that the horseshoe-shaped low-temperature patterns statistically appear at a fixed location in the transition region.

As illustrated in a series of figures, the time-and-space scales are statistically independent of both  $q_w$  ( $W m^{-2}$ ) and  $\overline{H}$  (m), when the data were ensemble-

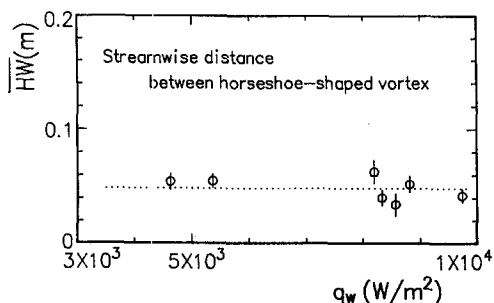


Fig. 19. Ensemble-averaged streamwise distance between vertically aligned horseshoe-shaped low-temperature patterns.

averaged. As pointed out by Jaluria and Gebhart [15], the modified Grashof number,  $Gr_H^*$ , has an insignificant influence in the spanwise velocity distribution. Therefore, we presumed that the present statistical quantities are independent of both  $q_w$  ( $W m^{-2}$ ) and  $\overline{H}$  (m).

We learned more about the character of the velocity and temperature fields through the thermal and flow visualizations. In particular, the clarification of the life span will be most important in developing the first stages of a structural modeling such as a surface renewal model [21–23]. The life span, e.g. the resident time of a large scale low-temperature pattern on the wall, was defined as a characteristic value in these surface renewal models.

Figures 21–25 show the histograms for the time-and-space scales of a horseshoe-shaped low-temperature pattern. From observing these histograms, we can easily understand their time-and-space distributions on the wall. As far as the authors know, the distributions of the time-and-space scales have not yet been discussed in the transition region.

#### 4. CONCLUDING REMARKS

Heat transfer and fluid flow of natural convection along a vertical flat plate was experimentally investigated in the transition region. Local heat transfer coefficients along a vertical flat plate were measured

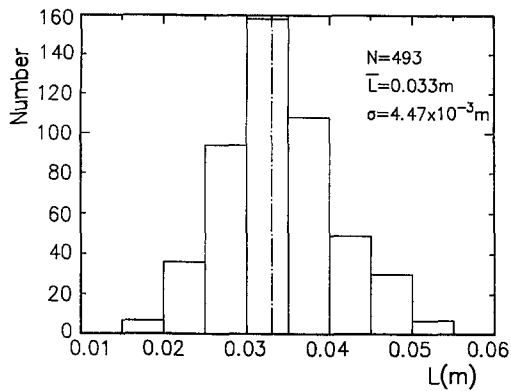


Fig. 22. Histogram for the streamwise length of a horseshoe-shaped low-temperature pattern.

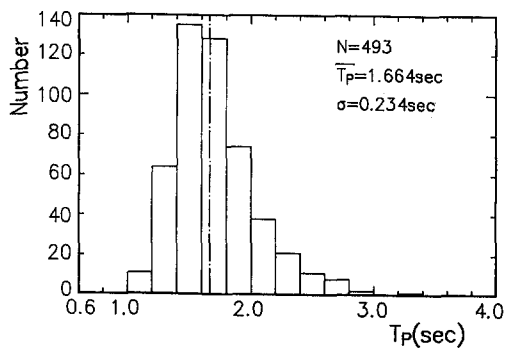


Fig. 23. Histogram for the passage time of a horseshoe-shaped low-temperature pattern.

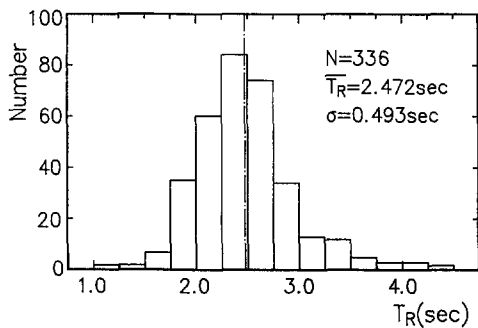


Fig. 24. Histogram for the life span of a horseshoe-shaped low-temperature pattern.

first to distinguish the transition region. The wall temperature and fluid flow were then visualized using a liquid crystal sheet and water-soluble fluorescent paint. The visualized patterns were analysed by a digital image processing unit connected to a personal computer. Moreover, we discussed the characteristic statistical quantities with the aid of visualizations for both the velocity and temperature fields.

It was revealed from the thermal visualization that horseshoe-shaped low-temperature patterns appear on the wall and that they play a significant role in heat transfer. It was then revealed from the flow visual-

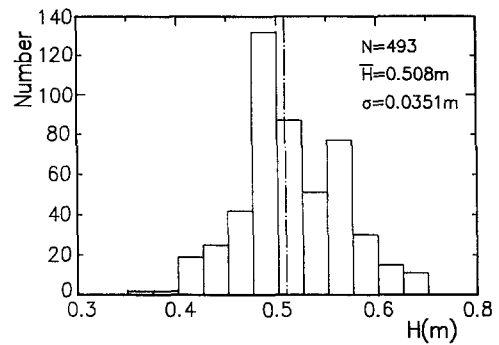


Fig. 25. Histogram for the occurring position of a horseshoe-shaped low-temperature pattern.

ization that the W-shaped flow patterns appear in the near-wall region and that they play a significant role in the laminar to turbulent transition. The W-shaped flow pattern possesses three-dimensional and unstable structures. By combining two types of visualizations, it was revealed that the low-temperature-and-velocity and high-temperature-and-velocity fluid motions are combined in this flow pattern. It was also revealed that a horseshoe-shaped low-temperature pattern is generated by a W-shaped flow pattern. When the data was ensemble-averaged it was found that the characteristic time-and-space scales of the horseshoe-shaped low-temperature patterns were statistically independent of not only heat flux but also occurring position. It will be necessary in future work to develop an appropriate modeling of natural convection in the transition region by measuring various fluctuating physical quantities.

## REFERENCES

1. R. Cheesewright, Turbulent natural convection from a vertical plane surface, *Trans. ASME Series C, J. Heat Transfer* **90**, 1-8 (1968).
2. G. C. Vliet and C. K. Liu, An experimental study of turbulent natural convection boundary layer, *Trans. ASME Series C, J. Heat Transfer* **91**, 517-531 (1969).
3. M. Miyamoto, H. Kajino, J. Kurima and I. Takanami, Development of turbulence characteristics in a vertical free convection boundary layer, *Proc. 7th International Heat Transfer Conference*, Vol. 2, pp. 323-328 (1982).
4. M. Miyamoto, H. Kajino, J. Kurima and I. Takanami, Development of turbulence characteristics in a vertical free convection boundary layer, *Proc. 18th National Heat Transfer Symposium of Japan*, pp. 295-297 (1981).
5. T. Fujii, M. Takeuti, M. Fujii, K. Suzaki and H. Uehara, Experiments on natural convection heat transfer from the outer surface of a vertical cylinder to liquids, *Int. J. Heat Mass Transfer* **13**, 753-783 (1970).
6. T. Tsuji and Y. Nagano, Characteristics of a turbulent natural convection boundary layer along a vertical flat plate, *Int. J. Heat Mass Transfer* **31**, 1723-1734 (1988).
7. T. Tsuji and Y. Nagano, Turbulent measurements in a turbulent natural convection boundary layer along a vertical flat plate, *Int. J. Heat Mass Transfer* **31**, 2101-2111 (1988).
8. T. Fujii, On the generation of a vortex street in the free convection boundary layer, *Trans. Japan Soc. Mech. Engng* **24**, 973-977 (1958).

